Oncogenic *NTRK3* mutations exhibit differential sensitivity to tropomyosin receptor kinase inhibitors in patients with acute myeloid leukemia

Genomic analyses of tumors have identified rare oncogenic aberrations in the neurotrophic receptor tyrosine kinase (NTRK) genes - *NTRK1, NTRK2, NTRK3* - encoding TrkA, TrkB, TrkC receptors, respectively.[1] Characterization of Trk oncoproteins in solid malignancies led to the Food and Drug Administration (FDA) approval of first-generation Trk inhibitors, larotrectinib[2] and entrectinib.[3] Second-generation Trk inhibitors, such as repotrectinib,[4] have been granted FDA breakthrough designation for patients failing first-line Trk inhibitors. Other inhibitors, such as selitrectinib[5] and taletrectinib,[6] are currently in clinical trials.

Beyond solid malignancies, there is a growing appreciation for Trk signaling in hematologic malignancies owing to the success of Trk inhibitors.[7] Similar to solid tumors, Trk fusions (e.g., *ETV6-NTRK3*) represent the primary genetic aberration that confer oncogenic behavior in Trk-driven liquid tumors.[7] Our laboratory previously identified four novel, *NTRK2* and *NTRK3* non-kinase domain point mutations in patients with leukemia. These mutations result in Trk activation via increased cell surface abundance and receptor dimerization and importantly are amenable to Trk inhibition.[8] Herein we characterize two additional novel *NTRK3* kinase domain point mutations, L568V and P792S, identified through exome sequencing of 805 acute myeloid leukemia (AML) patient samples via the Beat AML research program[9] (Figure 1A) with variant allele frequencies (VAF) of 26% and 32%, respectively. These specimens were collected with informed consent from patients with AML according to a protocol approved by the Oregon Health and Science University (OHSU) institutional review board (IRB #4422; NCT01728402). Both were confirmed via Sanger sequencing (Figure 1B, C).

Initially, both patients were diagnosed with myelodysplastic syndromes (MDS) prior to AML progression. Patient 2232, harboring $NTRK3^{P792S}$, transformed into AML after 7 months, received standard of care induction and consolidation, and remained in remission 1-year post-transplant but was lost to follow-up. Patient 4838 with $NTRK3^{L568V}$ was initially treated with lenalidomide and azacitidine but transformed to AML with the likely co-acquisition of *NRAS* and *NTRK3* mutations and died within 79 days despite a trial of palliative chemotherapy. A DNA sample during the MDS phase was available for this patient at approximately 135 days prior to AML transformation. Sequential sequencing efforts (*Online Supplementary Table S1*) revealed that the $NTRK3^{L568V}$ mutation was undetectable during MDS but arose during the evolution to AML (Figure 1D). Based upon the VAF, the $NRAS^{Q61H}$ and $NTRK3^{L568V}$ mutations appear to arise in the same clone. No DNA was available to perform a similar clonal analysis for patient 2232. Both patients exhibited similar co-occurring mutations including: *NRAS* mutations (Q61H for L568V and G12D for P792S), identical $IKZF1^{N159S}$ mutations, and *RUNX1* alterations (*Online Supplementary Table S1*; patient characteristics). While P792 is a conserved residue among receptor tyrosine kinases, the L568 residue is not, but is within an area of conserved residues (*Online Supplementary Figure S1A*).

Both *NTRK3* mutations conferred interleukin 3 (IL-3)-independent growth in Ba/F3 cells, while overexpression of $NTRK3^{wild\text{-}type(WT)}$ or $NTRK3^{I695T}$ did not (identified in TCGA,[10] TCGA-AB-2821; Figure 1E). Immunoblot analysis revealed increased total and phosphorylated TrkC expression in mutant-transformed Ba/F3 cells (Figure 1F).

To explore how *NTRK3* mutants activate TrkC, we performed molecular dynamic simulation (MDS) studies with the available crystal structure of the TrkC kinase domain[11] and homology modeling to fill in missing loop regions. We developed structural models of $NTRK3^{WT}$, $NTRK3^{L568V}$, and $NTRK3^{P792S}$ in their 'active' or aspartate-phenylalanine-glycine (DFG)-in and 'inactive' or DFG-out states to assess how the mutants altered the structure, stability, dynamics, or interactions of TrkC. Root mean square fluctuation (RMSF) analyses suggested that both mutants enabled an increase in local flexibility relative to $NTRK3^{WT}$, which was most pronounced in the TrkC inactive conformation (Figure 1G) relative to the active conformation (Figure 1H). Three regions were evaluated: region 1, containing L568 and encompassing the P-loop that interacts with ATP; region 2, a loop region proximal to P792 spatially; and region 3, encompassing the activation loop. Region 4 served as a negative control as it is mostly unperturbed in both mutants regardless of receptor conformation. MDS analyses revealed residue hyper-mobility within regions surrounding or encompassing the activation loop (i.e., region 2 and 3) as evident by the magnitude of fluctuation relative to the $NTRK3^{WT}$ baseline (denoted by dotted line; Figure 1G, H). $NTRK3^{L568V}$ showed an approximate 3-fold difference in local fluctuation at regions 2 and 3 in the inactive conformation. $NTRK3^{P792S}$ showed an approximate 6-fold difference in fluctuation. The enhancement in local flexibility resulted in increased pocket volume (Figure 1I-L) near the receptor activation site, which again was most prominent in the inactive TrkC conformation (Figure 1J, K). WT TrkC receptor in the inactive conformation had a pocket volume

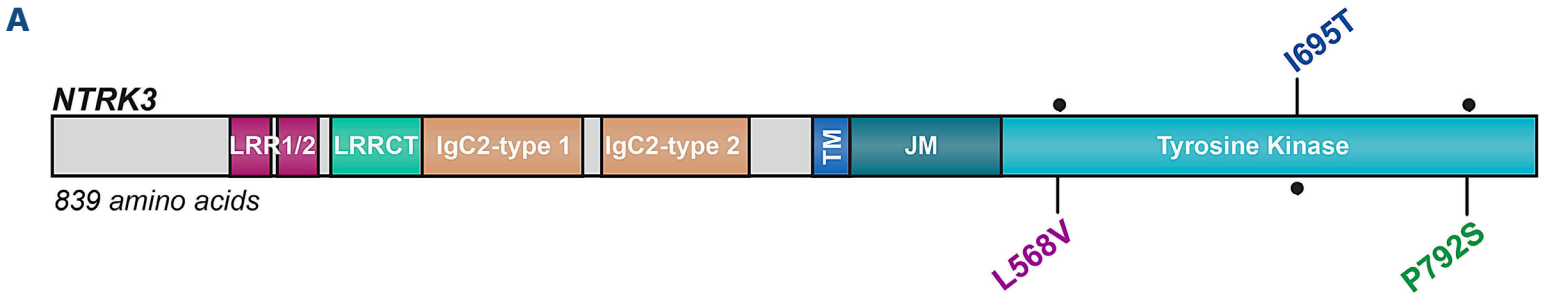

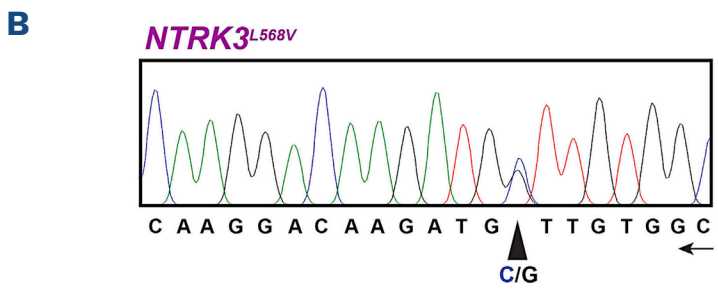

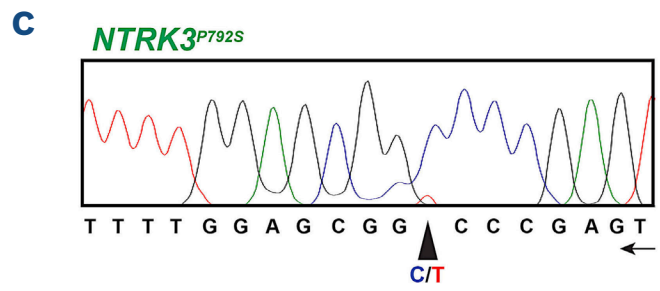

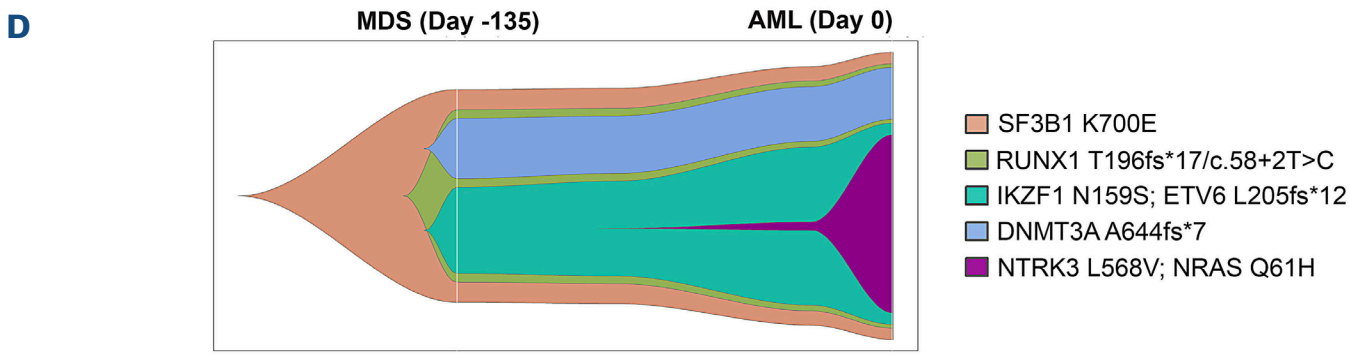

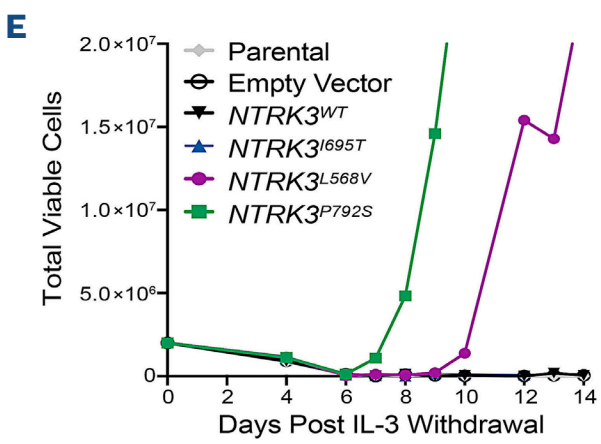

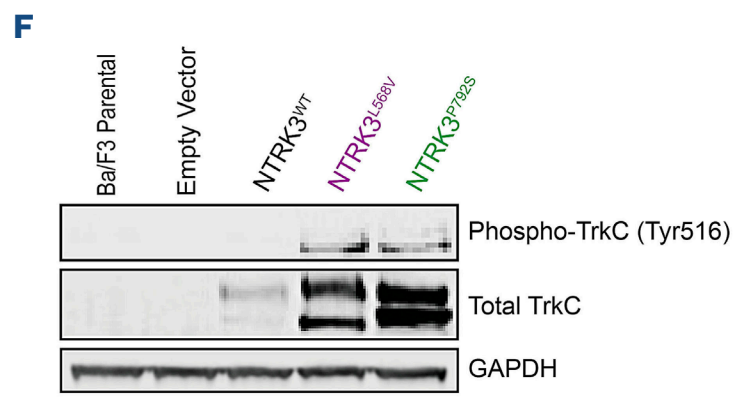

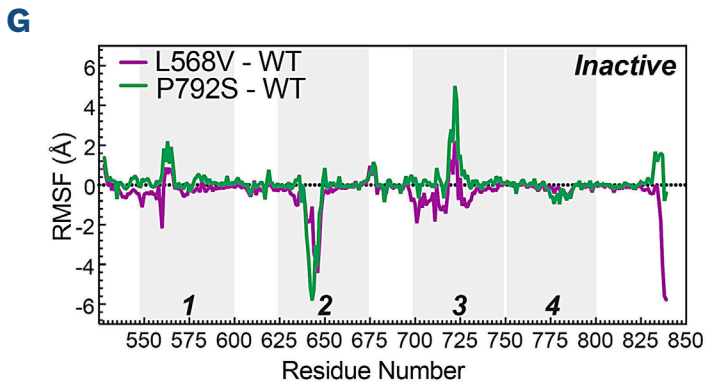

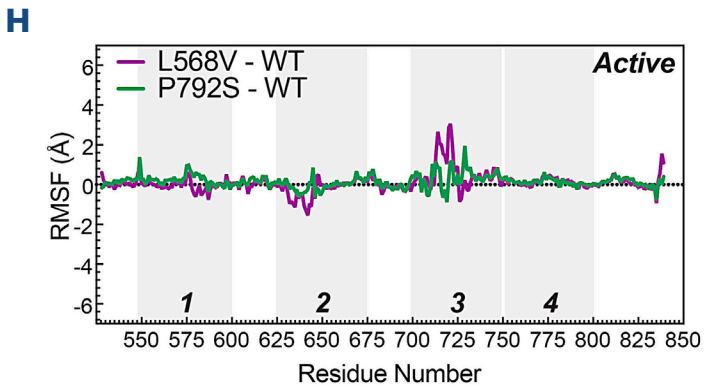

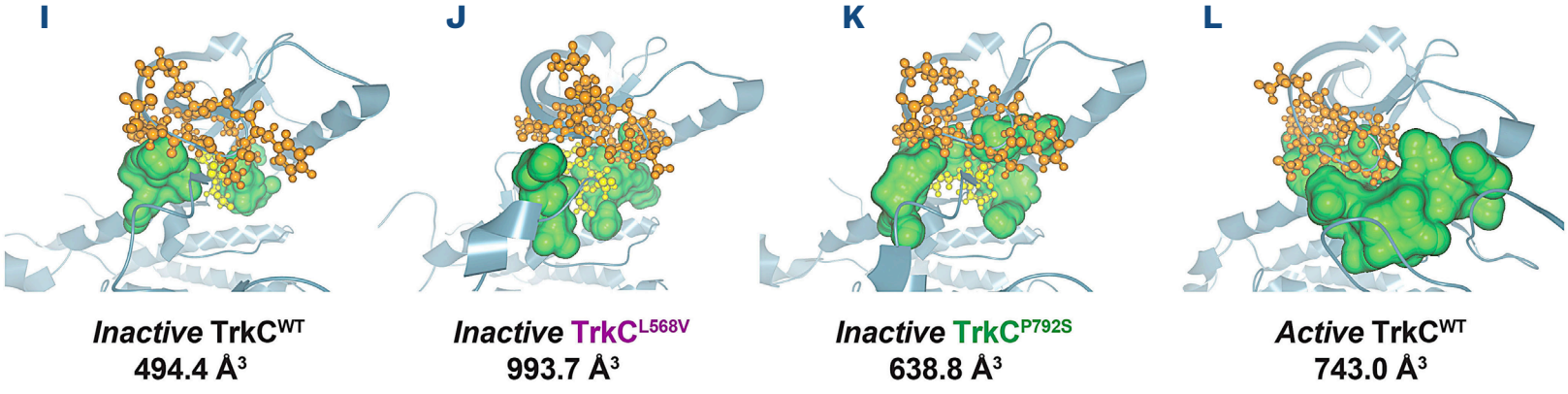

Continued on following page.

Figure 1. Point mutations found in acute myeloid leukemia patient samples alter local flexibility of the inactive receptor, enabling TrkC activation and oncogenicity. (A) Lollipop diagram depicts the location of *NTRK3* point mutations (below: Beat acute myeloid leukemia [AML]; above: TCGA). The locations of the following domains are included: LRR 1, LRR 2, LRRCT, Ig-like C2-type 1, Ig-like C2-type 2, transmembrane (TM), juxtamembrane (JM), and tyrosine kinase. (B, C) Electropherograms from Sanger sequencing of patient genomic DNA confirm the presence of $NTRK3^{L568V}$ and $NTRK3^{P792S}$ mutations. Peaks correspond to the following nucleotides: A (green), T (red), C (blue), and G (black). Arrows indicate direction of sequencing. (D) Fish plot illustrating evolution of $NTRK3^{L568V}$ from DNA isolated from bone marrow aspirate as captured by target panel DNA sequencing at myelodysplastic syndromes (MDS) stage (day -135) and at time of transformation to AML (day 0). Top x-axis indicates clinical time point. Clonal fractions are displayed as double the variant allele frequency (VAF), consistent with the assumption of heterozygous mutations without copy number variation except for *DNMT3A*, which is commonly biallelic and not doubled in this depiction. ETV6 and IKZF1 are presented as a single event, using the larger VAF of the pair, as the clonal order could not be resolved with data available. Similarly, the *NTRK3* and *NRAS* VAF are also presented as a single event. (E) $NTRK3^{L568V}$ and $NTRK3^{P792S}$ mutations transform the murine Ba/F3 pro-B-cell line and enable interleukin 3 (IL-3)-independent growth. No growth was observed in Ba/F3 cells harboring an empty vector (pMX-IRESpuro), wild-type (WT) *NTRK3*, or $NTRK3^{I695T}$. Total viable cells are plotted over time and cell growth was measured after the withdrawal of IL-3. This experiment was repeated at least twice with consistent results. (F) Expression of total and phosphorylated TrkC is increased in mutant-transformed Ba/F3 cells relative to WT cells. GAPDH served as a loading control. Prior to lysis, WT cells were grown in IL-3-supplemented media and all cell lines were starved overnight in 0.1% bovine serum albumin (BSA) RPMI. (G, H) MDS studies reveal differences in root mean square fluctuation (RMSF, Angstroms (Å)) between *NTRK3* mutations and WT in the active (aspartate-phenylalanine-glycine [DFG-in]) and inactive (DFG-out) TrkC conformations. Areas denoted in gray highlight regions of residues that exhibit fluctuation and/or served as a negative control for simulation studies. (I-L) Pocket volume size ($Å^3$) was measured as a surrogate to assess TrkC activation in both the inactive and active conformations. Increase in pocket volume was observed following the addition of *NTRK3* mutations in the inactive (DFG-out) conformation, denoting increased TrkC activation. Orange: ATP-binding loop; yellow: aspartate-phenylalanine-glycine (DFG) motif, DFG-in (active conformation), or DFG-out (inactive conformation); green: cavity to assess changes in pocket-volume size. For detailed methods see: https://doi.org/10.6084/m9.figshare.26516974.v4.

of 494.4 $Å^3$ (Figure 1I). This increased to 993.7 and 638.8 Å3 in the setting of L568V and P792S, respectively (Figure 1J, K). L558 is juxtaposed with the substrate binding site whereas P792 is located far from the substrate binding site and yet still affects inhibitor interactions. These mutant pocket volume sizes mirrored the active conformation of the WT receptor (743.0 $Å^3$; Figure 1L). Mechanistically, these structural studies implicate that both *NTRK3* mutants possibly perturb the inactive receptor to adopt the active conformation, thereby conferring increased kinase activity with resulting oncogenicity.

To further characterize the downstream impact of *NTRK3* mutations, we performed global, phospho-serine/threonine, and phospho-tyrosine enriched proteomic analyses on Ba/F3 cells expressing empty vector, $NTRK3^{WT}$, $NTRK3^{L568V}$, and $NTRK3^{P792S}$. All mutant-expressing cell lines clustered distinctly from $NTRK3^{WT}$, empty vector, Ba/F3 parental cell lines (Figure 2A). The number of unique genes is summarized in *Online Supplementary Table S1* (global summary). These data were used to decipher pathways uniquely up- or down-regulated in each mutant cell line (Figure 2B). Common pathways, such as oxidative phosphorylation and E2F targets, were highlighted for both mutants, respectively compared to $NTRK3^{WT}$. Each mutant also possessed unique pathways, such as fatty acid metabolism for $NTRK3^{L568V}$ and mitotic spindle for $NTRK3^{P792S}$. Gene set enrichment analysis (GSEA) brought forth upregulated terms associated with cell division (*Online Supplementary Figure S2A, B*). Kinase substrate enrichment analysis (KSEA) highlighted significant enrichment of PI3K/MTOR pathway substrates for $NTRK3^{L568V}$. Similar substrates were highlighted for $NTRK3^{P792S}$ but did not reach statistical significance (Figure 2C). Together these data support activation of canonical downstream TrkC signaling and reveal novel metabolic and catabolic pathways that may inform *NTRK3* L568V and $NTRK3^{P792S}$ activity.

We also assessed *ex vivo* sensitivity of primary cells available from patient 4838 harboring $NTRK3^{L568V}$ and compared this half-maximal inhibitory concentration (IC_{50}) to the median IC_{50} calculated for all patient samples tested with entrectinib.[9] Inhibitors with IC_{50} values <20% of the median IC_{50} are considered "effective".[12] The $NTRK3^{L568V}$ patient fell outside this threshold, demonstrating a modest sensitivity to entrectinib with an IC_{50} of 0.503 nM (Figure 3A). *Ex vivo* inhibitor data was not available for the patient harboring $NTRK3^{P792S}$. $NTRK3^{L568V}$-transformed Ba/F3 cells also exhibited decreased sensitivity to entrectinib (IC_{50}=120.2 nM) and larotrectinib (IC_{50}=375.8 nM; Figure 3B, C). Interestingly, $NTRK3^{P792S}$-Ba/F3 cells demonstrated robust sensitivity to both Trk inhibitors (IC_{50}=5.0 nM; larotrectinib and 1.3 nM; entrectinib). Both *NTRK3*-mutant-expressing Ba/F3 cell lines were sensitive to second generation Trk inhibitors - repotrectinib, selitrectinib, and taletrectinib (Figure 3D-F; all data summarized in *Online Supplementary Table S1*; inhibitor screen summary).

We investigated the differential sensitivity pattern of $NTRK3^{L568V}$ to Trk inhibitors via molecular docking studies by generating *in silico* models. We assessed larotrectinib and repotrectinib, two prototypical examples of first- and second-generation TrkC inhibitors, docked onto the active and inactive conformations of the TrkC kinase domain. Docking studies, including the dissociation constants calculated (*Online Supplementary Table S1*; dissociation constants docking experiments), were concordant with the trends observed in the cell-based IC_{50} data (Figure 3C, D). Repotrectinib had lower dissociation constants for both mutants compared to larotrectinib. We then analyzed the multiple interactions - hydrophobic, π-π, cation-π, and ionic - that facilitate binding between the WT or mutant

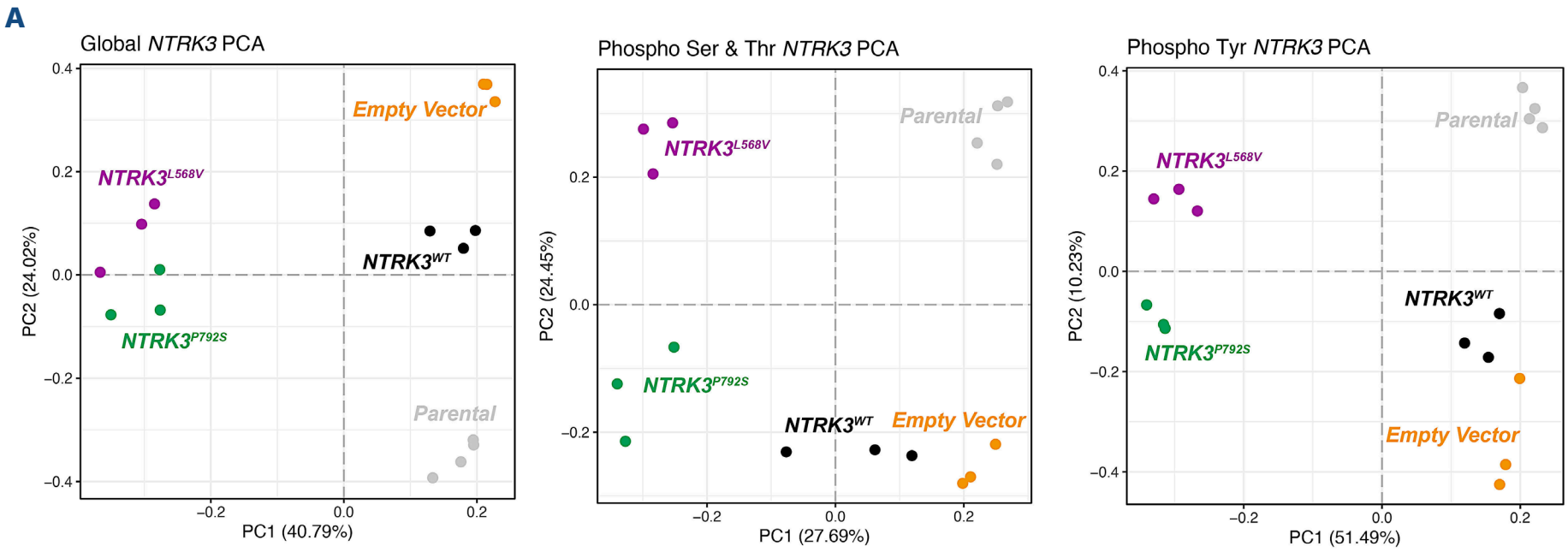

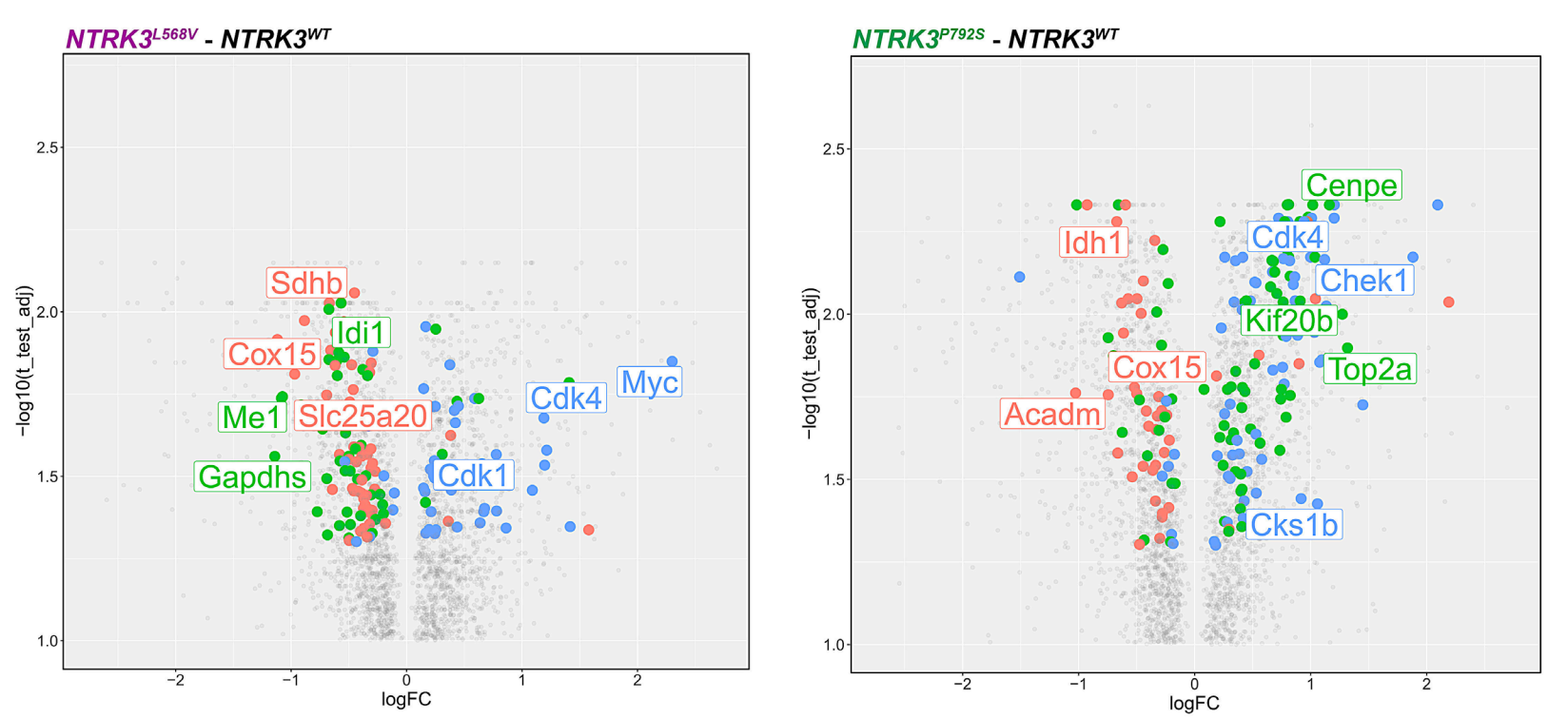

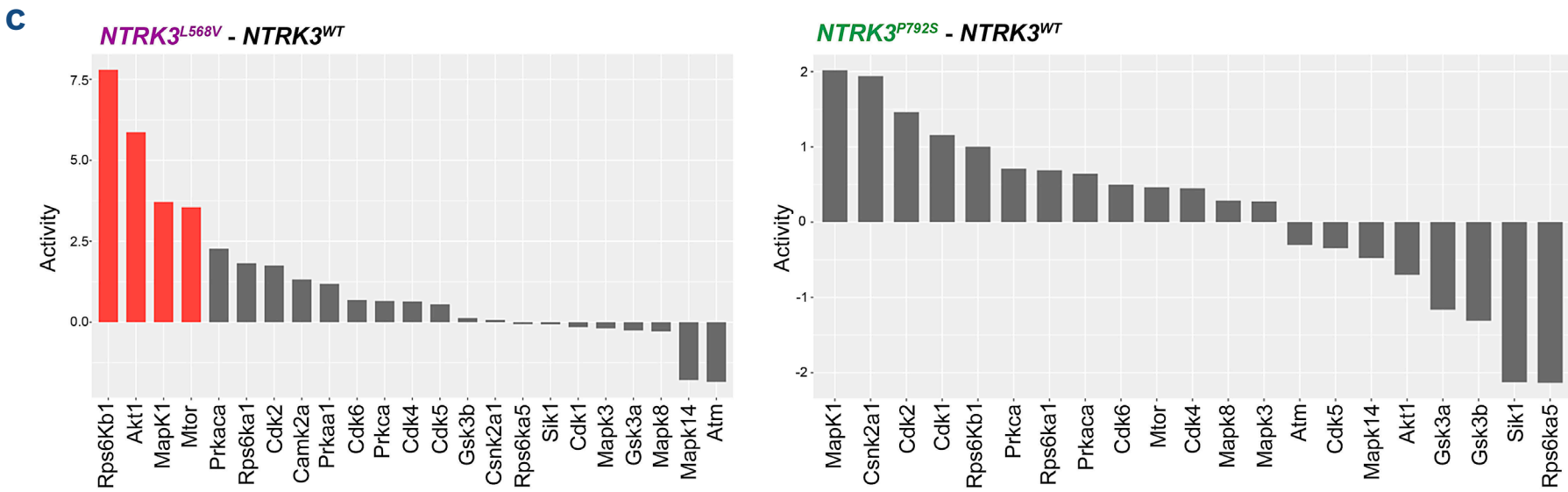

Figure 2. Proteomic analysis of *NTRK3* mutant-expressing Ba/F3 cells highlights activation of canonical downstream signaling pathways and alterations in metabolism. (A) Visualization of global proteomic (left), phospho-serine/threonine (middle) and phospho-tyrosine (right) profiling by principal component analysis (PCA) shows distinct clustering amongst parental, empty vector, *NTRK3*$^{wild\text{-}type(WT)}$, and *NTRK3* mutant-expressing cells. (B) Volcano plots depicting the significantly differentially expressed peptides identified in *NTRK3* mutant-expressing Ba/F3 cells as assessed by -log10 (*t* test adjusted) values. Peptides were annotated using the Hallmarks of cancer pathway analysis. Three pathways are highlighted for each mutant. (C) Kinase substrate enrichment analysis (KSEA) analyses reveal alterations in PI3K/AKT/MTOR and MAPK pathways in *NTRK3* mutant-expressing cell lines. Red bars =significantly upregulated kinase activity. Grey bar =not significant. For detailed methods see: https://doi.org/10.6084/m9.figshare.26516974.v4.

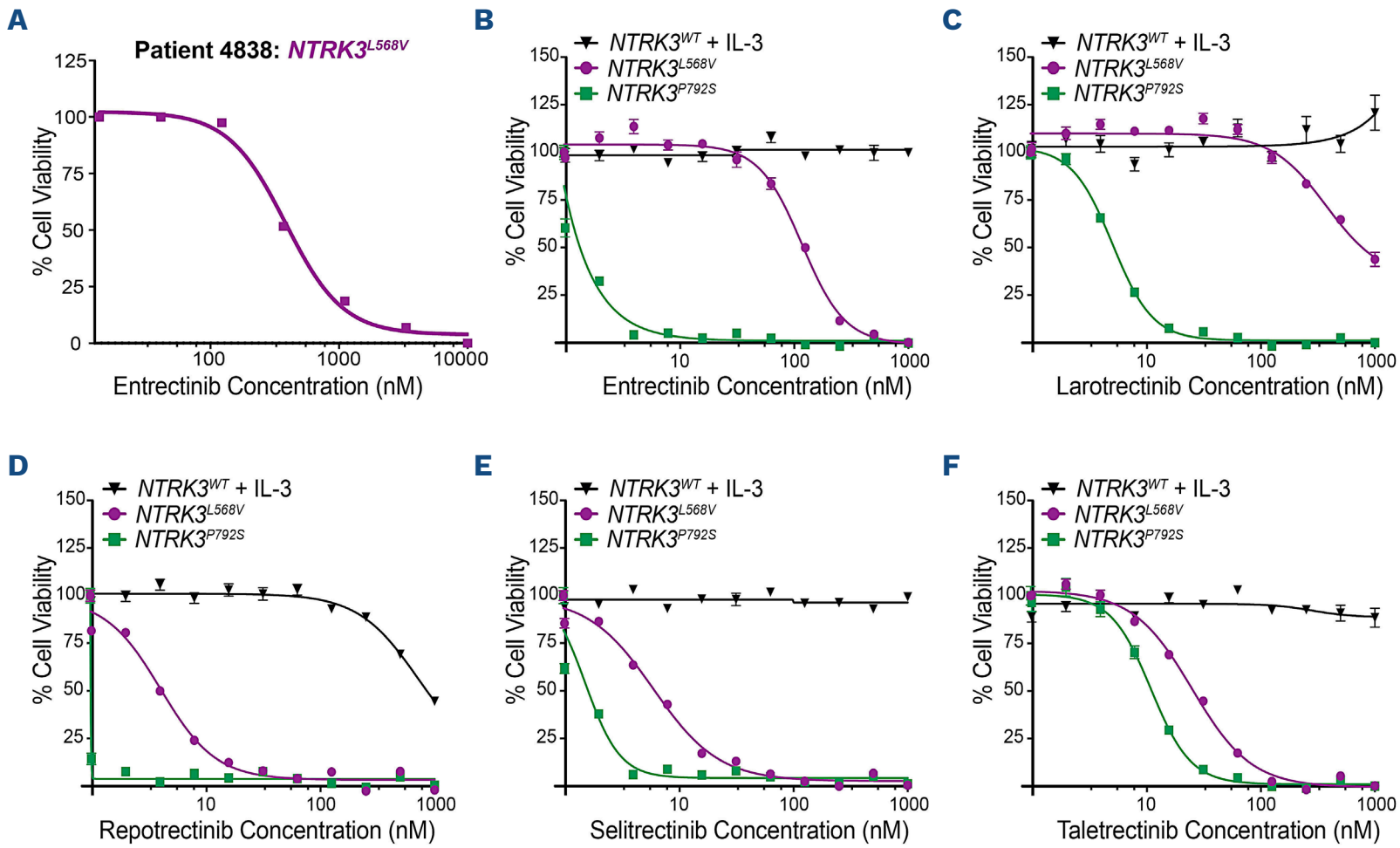

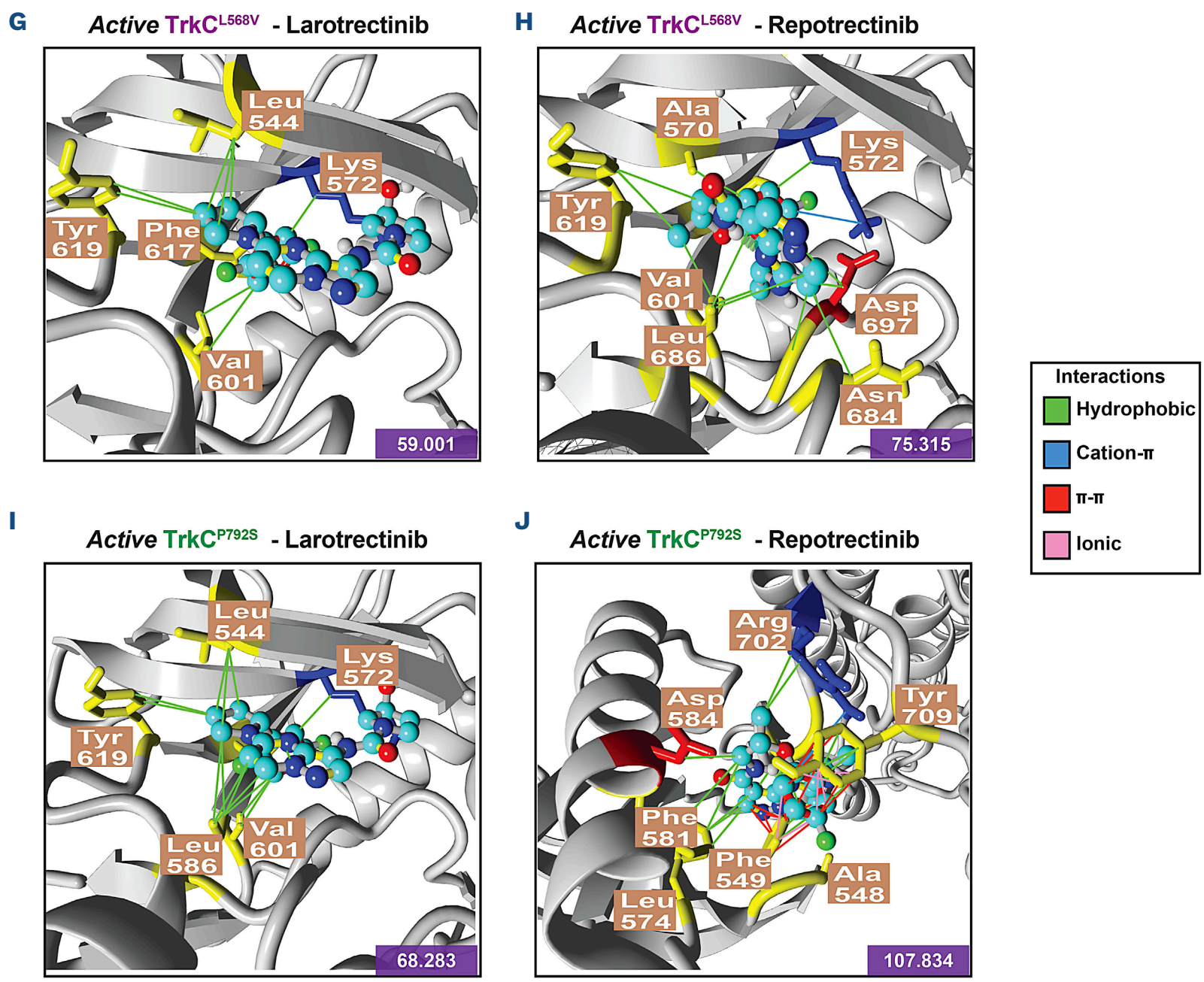

Continued on following page.

Figure 3. *NTRK3* mutants are unequivocally sensitive to second-generation Trk inhibitors owing to enhanced local interactions. (A) *Ex vivo* entrectinib sensitivity assay results from the primary acute myeloid leukemia (AML) patient sample harboring *NTRK3*^{L568V} from Beat AML data base. Freshly isolated mononuclear cells isolated from the bone marrow were incubated with increasing doses of entrectinib and assayed for viability after 3 days of incubation. Sensitivity was evaluated by calculating % median half-maximal inhibitory concentration (IC_{50}), which has historically been a marker for patient samples demonstrating sensitive to a given drug screened in the inhibitor assay.[9] (B-F) Six replicates of wild-type (WT) and mutant *NTRK3* Ba/F3 cells were plated with varying concentrations of entrectinib (B), larotrectinib (C), repotrectinib (D), selitrectinib (E), and taletrectinib (F) for 72 hours. *NTRK3*^{WT} cells were plated in media supplemented with interleukin 3 (IL-3). Cell viability was determined using a tetrazolamine-based viability assay. Viability is represented as a percentage of the untreated control. The average mean ± standard error of the mean (SEM) is shown. (G-J) Larotrectinib (G, I) and repotrectinib (H, J) were docked *in silico* on the active conformation (aspartate-phenylalanine-glycine [DFG-in)]of L568V- and P792S-mutated TrkC receptor to study extent of local interactions. Purple boxes at bottom right corner indicate aggregate interaction scores. A higher score correlates with enhanced interactions between TrkC receptor and respective inhibitor. Four different interactions are highlighted: hydrophobic (green), cation- π (blue), π-π (red), and ionic (pink). The cation-π interaction is formed by the proximity of a positively charged residue (Lys, Arg) with aromatic residues (Phe, Trp, and Tyr). Docking repotrectinib within the L568V- or P792S-mutated TrkC receptors, enables formation of the cation-π interaction that stems from the lysine residue at 572 and arginine at 702, respectively. In the case of both mutants, these positively-charged residues interact with a fluorinated phenyl group of repotrectinib, enabling formation of the cation-π interaction. The new cation-π interaction coupled with an increased number of hydrophobic, π-π, and ionic interactions enable repotrectinib to retain a single-digit nanomolar potency against both *NTRK3* mutations, which is not the case with larotrectinib. Notably, in the case of the *NTRK3*^{L568V} mutant, repotrectinib's potency exceeds that of entrectinib and larotrectinib by approximately 30 to 90 orders of magnitude, respectively (*Online Supplementary Table S1*). For detailed methods see: https://doi.org/10.6084/m9.figshare.26516974.v4.

receptors in the active conformation with larotrectinib and repotrectinib.

We focused on the active conformation of the TrkC receptor given that larotrectinib and repotrectinib are both type I Trk inhibitors and, therefore preferentially bind in the active, DFG-in conformation. A higher aggregate interaction score is reflective of better interactions against a given *NTRK3* mutant, which likely translates into increased Trk inhibition and decreased cell viability experimentally (*Online Supplementary Figure S1B, C;* Figure 3G-J). In the case of *NTRK3*^{L568V}, repotrectinib demonstrated enhanced binding with a cumulative interaction score of 75.3 compared to 59.0 observed with larotrectinib binding (Figure 3G, H). The higher affinity for repotrectinib is likely driven by increased hydrophobic and π-π interactions and the presence of a new cation-π interaction not seen with the binding of larotrectinib to the L568V mutant (Figure 3G, H). Although repotrectinib binds the active site of *NTRK3*^{P792S} in a different orientation than *NTRK3*^{L568V}, a similar trend was observed with interaction scores of 107.8 and 68.2 for repotrectinib and larotrectinib, respectively (Figure 3I, J). Taken together, perturbation of the *NTRK3* kinase domain not only alters its dynamicity but impinges its sensitivity to first-generation Trk inhibitors, most notably in the case of L568V.

Herein we characterized two *NTRK3* kinase domain mutations in patients with AML and confirmed their oncogenicity. Importantly, experimental validation and molecular docking studies demonstrate that both mutations exhibit differential sensitivity against first-generation Trk inhibitors but robust sensitivity against second-generation inhibitors. Although specific genetic aberrations have long been known to drive the development of various cancers, our work shows that a reliance on genomics alone serves as a bottleneck and limits the deployment of precise therapeutics. To this end, the development of cell-based models enables rigorous evaluation of small molecule inhibitor sensitivity and resistance, thereby informing clinical practice.

Authors

Sunil K. Joshi,[1,2,3] Ariane Huang,[2] Janét Pittsenbarger,[2] Ujwal Shinde,[4] Camilo Posso,[5] Paul D. Piehowski,[6] Sara J.C. Gosline,[7,8] Richard D. Press,[2,9] Marina A. Gritsenko,[7] Chelsea Hutchinson,[7] Karl K. Weitz,[7] Kevin Watanabe-Smith,[2,10] Nicola Long,[2] Karin D. Rodland,[2,7] Jeffrey W. Tyner,[2,3,11] Brian J. Druker[2,3] and Cristina E. Tognon[2,10]

[1]Department of Medicine, Division of Hematology, Stanford University School of Medicine, Stanford, CA; [2]Knight Cancer Institute, Oregon Health & Science University, Portland, OR; [3]Division of Hematology and Medical Oncology, Department of Medicine, Oregon Health and Science University, Portland, OR; [4]Department of Chemical Physiology and Biochemistry, Oregon Health and Science University, Portland, OR; [5]Biological Sciences Division, Pacific Northwest National Laboratory, Richland, WA; [6]Environmental and Molecular Sciences Division, Pacific Northwest National Laboratory, Richland, WA; [7]Biological Sciences Division, Pacific Northwest National Laboratory, Richland, WA; [8]Department of Bioengineering, Oregon Health and Science University, Portland OR; [9]Department of Pathology, Oregon Health and Science University, Portland, OR; [10]Division of Oncological Sciences, Oregon Health and Science University, Portland, OR and [11]Department of Cell, Development and Cancer Biology, Oregon Health and Science University, Portland, OR, USA

Correspondence:
C. E. TOGNON - tognon@ohsu.edu

https://doi.org/10.3324/haematol.2024.285572
Received: April 29, 2024.
Accepted: February 5, 2025.
Early view: February 13, 2025.

Disclosures

CET has received research support from Notable Labs and AstraZeneca. JWT has received research support from Acerta, Agios, Aptose, Array, AstraZeneca, Constellation, Genentech, Gilead, Incyte, Janssen, Kronos, Meryx, Petra, Schrodinger, Seattle Genetics, Syros, Takeda, and Tolero; and serves on the advisory board for Recludix Pharma. BJD discloses scientific advisory board membership at Adela Bio, Aileron Therapeutics (inactive), Therapy Architects/ALLCRON (inactive), Cepheid, DNA SEQ, Nemucore Medical Innovations, Novartis, RUNX1 Research Program; scientific advisory board membership at/stock holdership of Aptose Biosciences, Blueprint Medicines, Enliven Therapeutics, Iterion Therapeutics, GRAIL, Recludix Pharma; board of directors at/stock holdership of Amgen, Vincerx Pharma; board of directors at Burroughs Wellcome Fund and CureOne; joint steering committee of Beat AML LLS; advisory committee at Multicancer Early Detection Consortium; founder of VB Therapeutics; sponsored research agreement with Enliven Therapeutics and Recludix Pharma; clinical trial funding from Novartis and Astra-Zeneca; royalties from patent 6958335 (Novartis exclusive license) and OHSU and Dana-Farber Cancer Institute (one Merck exclusive license, one CytoImage, Inc. exclusive license, and one Sun Pharma Advanced Research Company non-exclusive license); US Patents 4326534, 6958335, 7416873, 7592142, 10473667, 10664967, 11049247. All other authors have no conflicts of interest to disclose.

Contributions

Study supervision by SKJ, BJD, CET. Conception and design by SKJ and CET. Development of methodology by SKJ, US and CET. Acquisition of data by SKJ, AH, JP, US, PDP, RDP, MAG, CH, KKW and NL. Analysis and interpretation of data (e.g., statistical analysis, biostatistics, computational analysis) by SKJ, AH, JP, US, CP, SJCG, KW-S and CET. Writing, review, and editing of the manuscript by SKJ, US, CP, PDP, SJCG, KR, JWT, BJD and CET.

Acknowledgments

We are extremely thankful to our patients for their time and precious tissue samples. We also thank the Oregon Health and Science University Massively Parallel Sequencing Shared Resource for exome sequencing and the Biophysics Shared Resources Core for support with MDS studies.

Funding

This work was supported by the Acquired Resistance to Therapy Network (ARTNet), National Institutes of Health (NIH), National Cancer Institute (NCI) grant U54CA224019, NCI's Office of Cancer Clinical Proteomics Research (CPTAC) under U01 CA271412, and the Cancer Target Discovery and Development Network grant U01CA217862. This work was additionally supported by the Mark Foundation for Cancer Research (to JWT) and the Silver Family Foundation (to JWT). SKJ is supported by the ARCS Scholar Foundation, The Paul and Daisy Soros Fellowship, and the National Cancer Institute (F30CA239335). PNNL is operated for the DOE by Battelle Memorial Institute under contract DE-AC05-76RL01830.

Data-sharing statement

A detailed description of the material and methods are available for download: https://doi.org/10.6084/m9.figshare.26516974.v4. Analysis scripts are on our github project repo: PNNL-Comp-Mass-Spec/NTRK-Experiment-19. All other data are provided in the manuscript.

References

1. Cocco E, Scaltriti M, Drilon A. NTRK fusion-positive cancers and TRK inhibitor therapy. Nat Rev Clin Oncol. 2018;15(12):731-747.
2. Drilon A, Laetsch TW, Kummar S, et al. Efficacy of larotrectinib in TRK fusion-positive cancers in adults and children. N Engl J Med. 2018;378(8):731-739.
3. Drilon A, Siena S, Ou SI, et al. Safety and antitumor activity of the multitargeted Pan-TRK, ROS1, and ALK inhibitor entrectinib: combined results from two phase I trials (ALKA-372-001 and STARTRK-1). Cancer Discov. 2017;7(4):400-409.
4. Drilon A, Ou SI, Cho BC, et al. Repotrectinib (TPX-0005) is a next-generation ROS1/TRK/ALK inhibitor that potently inhibits ROS1/TRK/ALK solvent- front mutations. Cancer Discov. 2018;8(10):1227-1236.
5. Drilon A, Nagasubramanian R, Blake JF, et al. A next-generation TRK kinase inhibitor overcomes acquired resistance to Prior TRK kinase inhibition in patients with TRK fusion-positive solid tumors. Cancer Discov. 2017;7(9):963-972.
6. Katayama R, Gong B, Togashi N, et al. The new-generation selective ROS1/NTRK inhibitor DS-6051b overcomes crizotinib resistant ROS1-G2032R mutation in preclinical models. Nat Commun. 2019;10(1):3604.
7. Joshi SK, Davare MA, Druker BJ, Tognon CE. Revisiting NTRKs as an emerging oncogene in hematological malignancies. Leukemia. 2019;33(11):2563-2574.
8. Joshi SK, Qian K, Bisson WH, et al. Discovery and characterization of targetable NTRK point mutations in hematologic neoplasms. Blood. 2020;135(24):2159-2170.
9. Bottomly D, Long N, Schultz AR, et al. Integrative analysis of drug response and clinical outcome in acute myeloid leukemia. Cancer Cell. 2022;40(8):850-864.e9.
10. Cancer Genome Atlas Research N, Ley TJ, Miller C, et al. Genomic and epigenomic landscapes of adult de novo acute myeloid leukemia. N Engl J Med. 2013;368(22):2059-2074.
11. Cui S, Wang Y, Wang Y, et al. Design, synthesis and biological evaluation of 3-(imidazo[1,2-a]pyrazin-3-ylethynyl)-2-methylbenzamides as potent and selective pan-tropomyosin receptor kinase (TRK) inhibitors. Eur J Med Chem. 2019;179:470-482.
12. Kurtz SE, Eide CA, Kaempf A, et al. Molecularly targeted drug combinations demonstrate selective effectiveness for myeloid- and lymphoid-derived hematologic malignancies. Proc Natl Acad Sci U S A. 2017;114(36):e7554-E7563.